JVSTB
JOURNAL OF VACUUM SCIENCE AND TECHNOLOGY B

Development of AlGaN-based graded-index-separate-confinement-heterostructure deep UV emitters by molecular beam epitaxy

Haiding Sun, Jeff Woodward, Jian Yin, Adam Moldawer, Emanuele F. Pecora et al.

Citation: J. Vac. Sci. Technol. B **31**, 03C117 (2013); doi: 10.1116/1.4796107
View online: http://dx.doi.org/10.1116/1.4796107
View Table of Contents: http://avspublications.org/resource/1/JVTBD9/v31/i3
Published by the AVS: Science & Technology of Materials, Interfaces, and Processing

Development of AlGaN-based graded-index-separate-confinement-heterostructure deep UV emitters by molecular beam epitaxy

Haiding Sun, Jeff Woodward, Jian Yin, Adam Moldawer, Emanuele F. Pecora, Alexey Yu. Nikiforov, Luca Dal Negro, and Roberto Paiella
Department of Electrical and Computer Engineering and Division of Materials Science and Engineering, Photonics Center, Boston University, Boston, Massachusetts 02215

Karl Ludwig, Jr.
Department of Physics, Boston University, Boston, Massachusetts 02215

David J. Smith
Department of Physics, Arizona State University, Tempe, Arizona 85287

Theodore D. Moustakas[a)]
Department of Electrical and Computer Engineering and Division of Materials Science and Engineering, Photonics Center, Boston University, Boston, Massachusetts 02215

(Received 11 December 2012; accepted 8 March 2013; published 21 March 2013)

The authors report on the growth, structure, and emission properties of AlGaN double heterostructures having a graded-index-separate-confinement-heterostructure design. These devices were grown on the Si-face of 6H-SiC substrates by plasma-assisted molecular-beam epitaxy. The active region of the device consists of 75-nm thick $Al_{0.72}Ga_{0.28}N$ film, confined by two 50-nm thick compositionally graded $Al_xGa_{1-x}N$ films ($x = 1$–0.8 and $x = 0.8$–1) and two AlN cladding layers. X-ray diffraction and transmission electron microscopy provide evidence that the compositionally graded AlGaN layer may also be serving as a strain transition buffer, by blocking threading defects in the vicinity of the AlN/AlGaN heterointerface. Polarization dependent photoluminescence studies indicate that the emission from these structures at 257 nm is transverse magnetic polarized. Simulation studies indicate that the vertical confinement of the optical mode in these structures is 32.5% and simulations of the band structure indicate the formation of a *p-n* junction resulting from polarization-induced doping. Electron-beam pumping of these structures provides evidence of the onset of stimulated emission at room temperature. © *2013 American Vacuum Society*. [http://dx.doi.org/10.1116/1.4796107]

I. INTRODUCTION

AlGaN alloys are well suited for the development of ultraviolet (UV) optoelectronic devices (emitters, detectors, and optical modulators) because their energy gap can be tuned by changing the alloy composition to cover the UV electromagnetic spectrum from 210 to 360 nm.[1–3] Such semiconductor devices are expected to be lightweight, compact, and have low power requirements. In addition, nitride semiconductors are physically robust, chemically inert, have high corrosion resistance, and are non-toxic. These properties make them also attractive for use in hostile environments and at high temperatures.

Ultraviolet light emitters (LEDs, lasers), in particular, are crucial for a number of applications such as water purification, air/food sterilization, surface disinfection, free-space non–line-of-sight communication, epoxy curing, counterfeit detection, and fluorescence identification of biological/chemical agents. However, despite intense efforts worldwide, the maximum external quantum efficiency (EQE) of fully packaged AlGaN-based deep-UV LEDs emitting below 280 nm is only 1–3%.[4–7] Recently, Shatalov and co-workers[8] reported a UV LED emitting at 278 nm with EQE of 10%. This was accomplished through optimization of the extraction efficiency and packaging. This rather poor EQE is to be contrasted with InGaN-based violet-blue LEDs, whose EQE is about 50%.[9]

The development of UV semiconductor lasers is at an even earlier stage. Some groups have demonstrated optically pumped deep-UV lasers based on AlGaN multiple quantum well (MQW) structures emitting at 241 nm (Ref. 10) and 267 nm (Ref. 11) with room temperature threshold powers of 1.2 MW/cm^2 and 126 kW/cm^2, respectively. Furthermore, maximum net modal gain of $118 \pm 9\,cm^{-1}$ at 255 nm with very low transparency threshold of $5 \pm 1\,\mu J/cm^2$, which corresponds to $1.4 \times 10^{17}\,cm^{-3}$ excited carriers, was obtained by the introduction of deep potential fluctuations in the AlGaN wells.[12,13] However, the development of electrically pumped deep-UV semiconductor lasers is lagging due to the difficulty of *n*- and *p*-type doping of AlGaN alloys with high AlN mole fraction. This is due to the high ionization energies of Mg-acceptors and Si-donors, which are 630 and 280 meV, respectively, for AlN.[14,15] The reported shortest wavelengths of electrically pumped UV lasers are 342 and 336 nm with threshold currents of 8 and 17 kA/cm^2, respectively.[16,17]

Thus, any breakthrough in developing an electrically pumped deep-UV semiconductor laser will depend on our ability to efficiently dope AlGaN alloys p-type. A number of approaches have been proposed toward this goal. These include, for example, the use of alternative acceptors, such as substitutional beryllium[18] or interstitial fluorine,[19] the use of polarization enhanced AlGaN/GaN short period

a)Electronic mail: tdm@bu.edu

superlattices,[20,21] and the employment of delta-doping.[22] However, none of these approaches has led to efficient *p*-type doping of AlGaN alloys with high AlN mole fraction. An alternative approach to *p*-type doping of AlGaN alloys is polarization enhanced doping in compositionally graded AlGaN alloys.[23] In this method, 3D mobile carriers can be produced with the aid of polarization charges in graded AlGaN structures without any impurities. Application of these polarization enhanced doping layers has already been implemented in light emitting diodes and heterostructures using compositionally graded AlGaN alloys with small AlN mole fraction ($x < 0.3$).[24–26]

A semiconductor laser design, which can take advantage of the polarization-enhanced doping in compositionally graded AlGaN alloys, is the graded-index-separate-confinement-heterostructure (GRINSCH). Such a laser structure has been successfully implemented in the traditional cubic III-V semiconductors using either parabolic or linearly graded alloy compositional profiles for the confinement of carriers and the optical mode. Such designs led to lasers operating at very low current threshold.[27–29] However, it should be stressed that due to their cubic symmetry, polarization-enhanced doping is not present in the compositionally graded wave guiding layers of the GRINSCHs based on these III-V materials.

In this paper, we report our initial efforts to develop a GRINSCH double heterostructure emitter based on AlGaN alloys, designed to emit in the deep-UV region of the electromagnetic spectrum.

II. EXPERIMENT METHODS

A. Materials and device growth

The AlGaN-based GRINSCH double heterostructures were grown by plasma-assisted molecular-beam epitaxy (PA-MBE) on the Si-face of (0001) 6H-SiC substrates. The MBE system is equipped with an EPI Unibulb rf plasma source for nitrogen activation and traditional effusion cells for the evaporation of Al, Ga, and In. The substrate temperature during growth was monitored with a thermocouple placed in the cavity behind the substrate. The temperature was also measured with a pyrometer and it was found to be significantly lower. However, it should be stressed that neither of these two temperature measurements indicates the actual temperature of the growing film. The substrate preparation and film growth were monitored by reflection-high-energy-electron diffraction (RHEED) using 10 kV acceleration voltage. The SiC substrates were first carefully cleaned *ex situ* in organic solvents followed by dipping into heated piranha and then buffered Hydrofluoric acid to remove surface contaminants and oxides. In addition, the substrates were cleaned *in situ* by exposure to Ga flux at 750 °C for complete Ga coverage followed by fast heating to 850 °C for Ga desorption. This process was found to lead to a sharp RHEED pattern, which is attributed to the removal of oxygen, carbon, hydrogen, and other physisorbed or chemisorbed impurities through the formation of volatile Ga-compounds.

One important aspect for epitaxial growth of nitride alloys by PA-MBE on the Si-face of SiC substrates is avoidance of the formation of amorphous SiN by the reaction of the active nitrogen produced by the plasma source with the surface of SiC. To address this potential problem, we followed a method suggested first by Okumura and co-workers.[30,31] We deposited first a few monolayers of Ga to cover the SiC surface at 800 °C (the pyrometer reading was 680 °C) and then activated and stabilized the plasma source and initiated the AlN growth. Following this step, we ramped the substrate temperature to 880 °C (the pyrometer reading was 725 °C) to grow the rest of the AlN film. If any active nitrogen leaks around the shutter during the activation and stabilization of the plasma, it will form a few monolayers of GaN, which protects the surface of SiC from converting into SiN.

As in any heteroepitaxy, the growth of AlN on SiC proceeds via the formation and coalescence of islands. These islands tend to be small due to the high chemical affinity of Al for N. This growth mode leads to AlN films with columnar microstructure. In general, threading defects, in heteroepitaxially grown nitride semiconductors at relatively low temperatures, occur primarily at the boundaries of the domains due to incomplete coalescence of the islands.[32–34] Ga was also employed as a surfactant during AlN growth in order to improve the microstructure of the films. An additional potential advantage of using Ga as a surfactant during growth of AlN is the reduction of oxygen incorporation into the films.[35,36] This is because oxygen reacts with Ga and forms volatile GaO species.

The investigated device structure is shown schematically in Fig. 1. It consists of 500-nm AlN cladding layer, followed by 50-nm $Al_xGa_{1-x}N$ film graded linearly from $x = 1$ to $x = 0.8$. The active region of the device consists of 75 nm of $Al_{0.72}Ga_{0.28}N$, followed by the 50-nm $Al_xGa_{1-x}N$ graded linearly from $x = 0.8$ to $x = 1$ and 100 nm AlN cladding layer. Gallium and indium were used as surfactants during growth of the various layers in order to improve their crystal quality. In particular, the active region was grown under Ga-rich conditions, a growth mode that promotes the development of deep band structure potential fluctuations.[35–40] Such

FIG. 1. (Color online) Schematic of the investigated GRINSCH double heterostructure.

band-structure potential fluctuations result in localization of the injected excitons even at room temperature, which prevents them from diffusing and recombining nonradiatively at extended and point defects. As discussed in Refs. 35–40, such band-structure potential fluctuations lead to quantum wells and LEDs with internal quantum efficiency as high as 70%.[40]

B. Materials and device characterization

The surface morphology was studied by secondary electron microscopy (SEM) and atomic force microscopy (AFM). The structure and microstructure of the films and devices were investigated by x-ray diffraction (XRD) and transmission electron microscopy (TEM). On-axis θ-2θ XRD scans and off-axis reciprocal lattice maps were performed using a Philips four-circle high-resolution diffractometer. The TEM studies were carried out on cross-sectional samples that were prepared by standard mechanical polishing followed by ion-beam-thinning at 4.5 keV. Conventional diffraction-contrast images and high-resolution phase-contrast images were recorded with a JEM 4000EX high-resolution electron microscope equipped with a top-entry and double tilt specimen holder operated at 400 keV.

The optical properties of this set of structures have been investigated under optical pumping. The samples were excited with 220-nm, 150-fs laser pulses obtained by pumping a proper crystal (Spectra Physics GWU-24FL) with a mode-locked ultrafast high-power Ti:sapphire laser (Spectra Physics MaiTai, 82 MHz) operating at 880 nm. The laser pulses were focused on the sample surface through a cylindrical lens. The pumping fluence on the sample was 60 μJ/cm^2. Photoluminescence was collected from the cleaved edge of the sample through a UV-transmitting objective, a UV-transmitting movable analyzer, a computer-controlled f/4 monochromator (Cornerstone 260) with UV-efficient gratings, and a lock-in amplifier (Oriel Merlin) coupled to a UV-optimized photomultiplier tube (Oriel Instruments 77348).

The optical properties of the GRINSCH were also investigated by electron beam excitation at room temperature in a JEOL JSM-6100 SEM fitted with an Oxford Research Cathodoluminescence (CL) setup equipped with a Gatan Mono CL2 system. The electron-beam current was varied from 10 nA to 4 μA at an acceleration voltage of 10 kV. The surface and edge CL emission were collected using a parabolloidal mirror to a photomultiplier, and the excitation was done in the scanning mode.

III. RESULTS AND DISCUSSION

A. Simulation of optical confinement and band structure

The transverse magnetic (TM) polarized optical-mode confinement in the GRINSCH double structure, described in Fig. 2, was determined using a commercially available simulation tool (Comsol Multiphysics). Figures 2(a) and 2(b) show the near-field profile of the optical mode and the vertical profile of the index of refraction and optical mode, respectively. Refractive indices at an emission wavelength of 257 nm of 2.3766, 2.4684, and 2.70439–0.3277x ($0.8 \leq x \leq 1$)

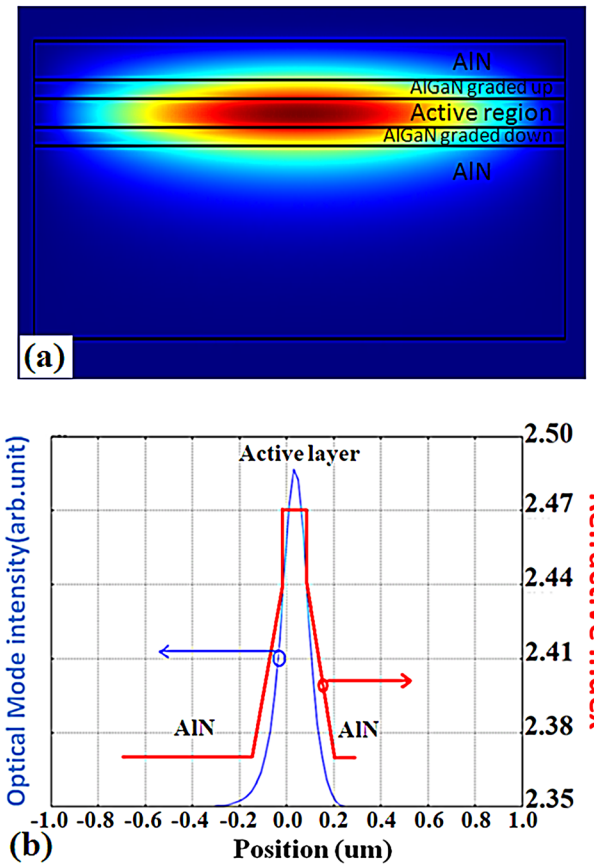

FIG. 2. (Color online) (a) Near field profile of the optical mode; (b) refractive index profile and calculated intensity of the optical mode.

were used for the AlN, $Al_{0.72}Ga_{0.28}N$, and graded $Al_xGa_{1-x}N$ layers, respectively.[41] As illustrated by the calculated transverse mode profile in Fig. 3(b), the optical mode was well confined by the graded AlGaN film, with an optical confinement factor, Γ, in the active region of the device of 32.5%, which is a significant improvement over the reported 1–3% for most InGaN and AlGaN MQW-based lasers.[16,42]

The energy band diagram, of the device described in Fig. 1, was found by solving self consistently the Schrodinger and

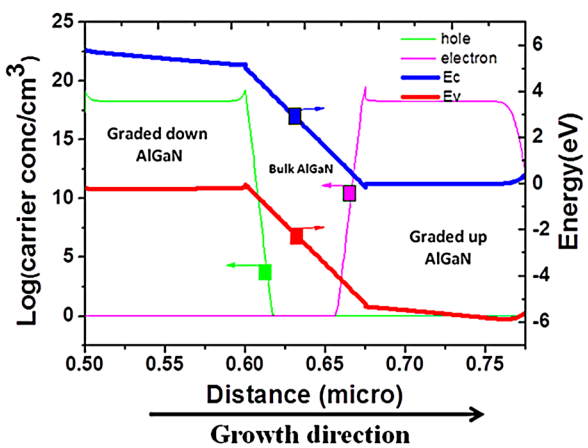

FIG. 3. (Color online) Simulated energy band diagram of the investigated GRINSCH. The polarization induced free carrier concentration in the p- and n-sides of the junction are also shown in this figure.

Poisson's equations, and the results are shown in Fig. 3. These calculations were done using a commercially available software package (Crosslight LASTIP). This band structure clearly indicates the formation of a *p-n* junction due to polarization n- and p-type doping of the AlGaN graded layers on either side of the active region.[23,24] In Fig. 3, we also show the free carrier concentration in the p- and n-sides of the junction. It should be stressed that this level of doping ($\sim 10^{18}\,\mathrm{cm}^{-3}$) was obtained without the use of dopants. Thus, this GRINSCH has the potential for the development of deep UV electrically pumped lasers.

In the rest of this paper, we discuss the growth, structure, and optical properties of this device as a deep-UV emitter, but without the use of a cavity, which is required for demonstration of lasing.

B. Film and device growth

Figures 4(a) and 4(b) show RHEED patterns recorded along the [10-10] and [11-20] azimuths of a 6H-SiC substrate after the *ex situ* and *in situ* surface preparation, which was discussed in Sec. II. The observed 3×1 surface reconstruction is evidence of good 6H-SiC surface preparation.

Figures 4(c) and 4(d) show the RHEED patterns for an AlN film grown on a 6H-SiC substrate. The bright and streaky RHEED patterns are both indicative of smooth AlN films. Moreover, the 2×2 surface reconstruction observed after the growth is evidence that the film has grown along the [0001] direction.

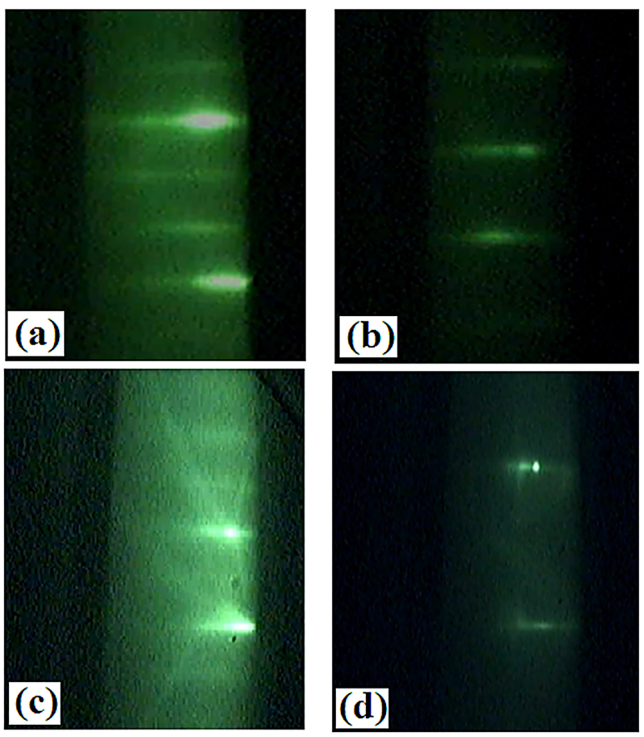

FIG. 4. (Color online) RHEED patterns of 6H-SiC substrate along (a) (1-100) and (b) (11-20) azimuths showing 3×1 reconstruction; RHEED pattern of the grown AlN film along (c) (11-20) and (d) (1-100) azimuths showing 2×2 surface reconstruction.

C. Crystal structure and microstructure

The surface morphology of the investigated GRINSCH was studied by SEM and AFM, and the crystal structure and microstructure were investigated by on-axis XRD, off-axis reciprocal lattice mapping, and TEM imaging.

Figure 5(a) shows a $2 \times 2\,\mu$m AFM image indicating that the RMS roughness of the sample is 0.79 nm. Optical microscopy images of the sample (not shown in this paper) show no evidence of cracks. Figure 5(b) shows a cross-section SEM image of the entire device structure cleaved along the (10-10) face (m-plane). These data indicate that formation of mirror laser facets by cleaving will be possible in these structures.

Figure 6(a) shows the on-axis XRD θ-2θ scan of the GRINSCH. The Al-content of the active region was determined by XRD to be 68%, which is smaller than the content determined from beam fluxes during growth (72%). This is the result of compressive strain as confirmed by the intensity contour plot around the (10-15) reciprocal lattice point shown in Fig. 6(b). These data indicate that the AlN cladding layer is partially relaxed with respect to the SiC substrate, while the AlGaN active region is likely to be coherent to the $Al_{0.8}Ga_{0.2}N$ of the graded AlGaN wave guiding layer. Detailed x-ray studies of AlGaN films can be found in a recent reference by Dalmau *et al.*[43]

Figure 7 shows a cross-sectional electron micrograph, recorded close to the [11-20] projection, of the GRINSCH.

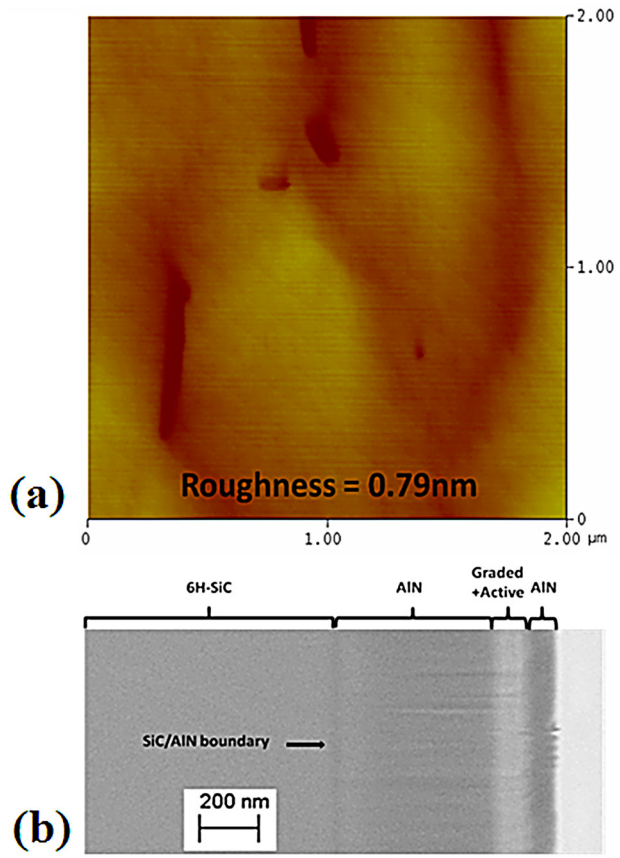

FIG. 5. (Color online) (a) AFM image of the surface morphology; (b) SEM cross section image of the investigated GRINSCH.

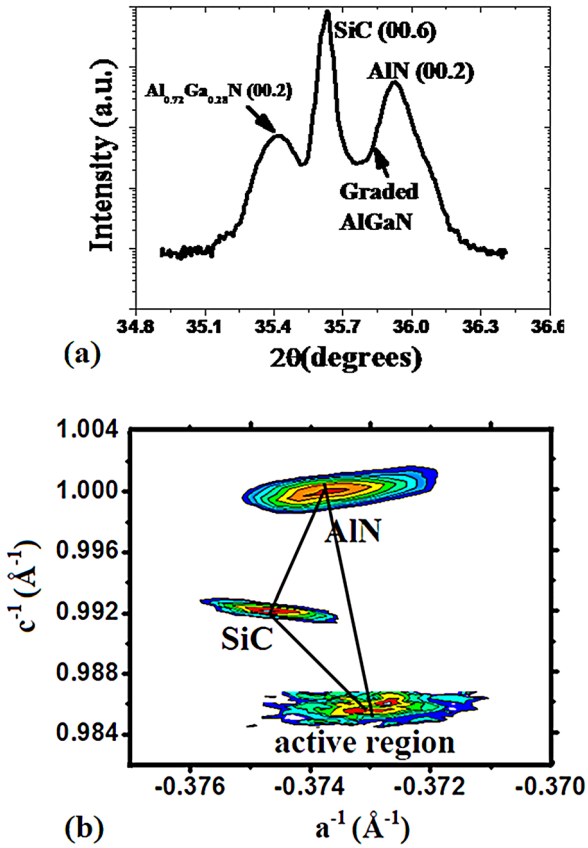

FIG. 6. (Color online) (a) XRD θ-2θ scan and (b) the reciprocal lattice map of the (-1015) reflection of the investigated GRINSCH.

Dense threading dislocations (TDs) were formed at the nucleation interface between AlN and SiC and propagate along the growth direction. Threading dislocation loops and annihilation in some areas of the sample is obvious (zone 1), while other TDs propagated through the AlN film (zone 2). However, many of the TDs terminate at the AlN/graded AlGaN layer, as shown in the enlarged image at the right. The likely cause for the dislocation termination at this interface is the strain associated with the compositionally graded

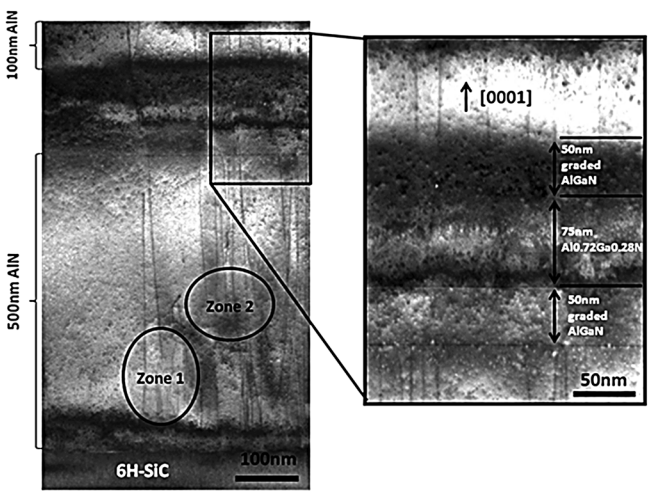

FIG. 7. TEM cross sectional micrograph of the GRINSCH, as recorded close to the [11-20] projection.

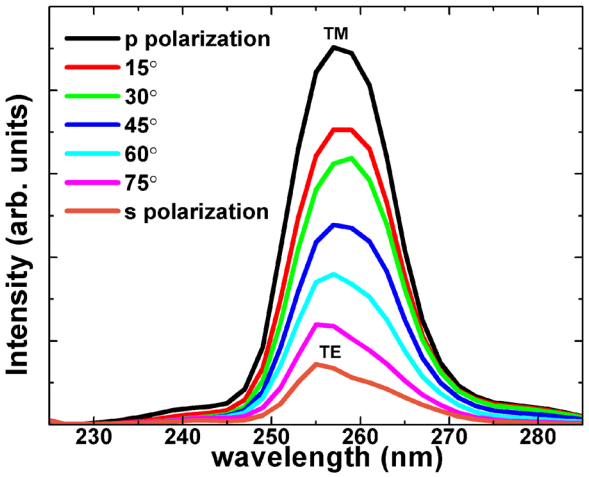

FIG. 8. (Color online) Polarization dependent PL spectra at different analyzer angles.

AlGaN wave guiding film. Thus, the graded AlGaN film not only provides strong optical and carrier confinement, but it also relieves strain between the cladding AlN layer and the active layer by serving as a strain transition buffer. These results indicate that the compositionally graded AlGaN layer with an optimum thickness and growth conditions can effectively block the TDs in the vicinity of the AlN/AlGaN heterointerfaces and reduce the density of TDs present in the active layer. Growth under these conditions leads to defect densities in the epitaxial structures estimated to be about 10^8 cm^{-2}, as reported previously.[12]

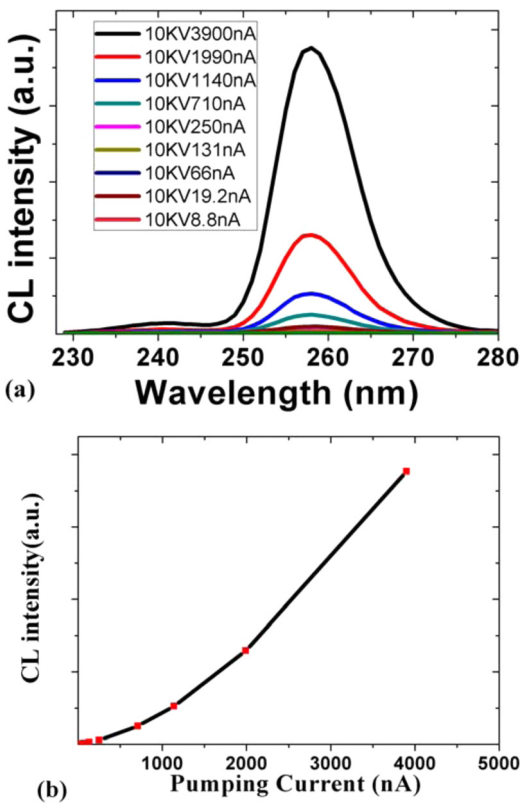

FIG. 9. (Color online) (a) CL Spectra under different pumping currents; (b) CL intensity vs pumping current.

D. Optical properties

The PL spectra, shown in Fig. 8, were collected from the edge of the sample at different angles, α, of the analyzer in order to investigate the polarization properties of the emitted light. The highest signal was measured for $\alpha = 0°$, corresponding to p polarization (TM mode). The PL signal decreased monotonically as soon as the angle α was increased, and eventually had its minimum for $\alpha = 90°$, corresponding to s polarization (TE mode). Thus, the emitted light is strongly TM polarized, and the degree of polarization, $P = (I_{TM} - I_{TE})/(I_{TE} + I_{TM})$, was measured by taking the integrated intensity under the spectra and found to be 0.79. Such a result is expected for bulk AlGaN films with 70% AlN mole fraction.[44] Optical gain measurements on these device structures will be reported elsewhere.[45]

The optical properties were also investigated by electron-beam pumping at an accelerating voltage of 10 kV and electron-beam current varying from 10 nA to 4 μA. The spectra show a single symmetric peak at 257 nm with a superlinear increase in the CL intensity of the emitted light [see Figs. 9(a) and 9(b)]. These results provide evidence of the onset of stimulated emission in these GRINSCH at room temperature.

IV. SUMMARY AND CONCLUSIONS

In conclusion, we have reported on the MBE growth and characterization of deep-UV-emitting AlGaN double heterostructure in the form of a GRINSCH configuration. Simulation results indicate that the compositionally graded AlGaN wave-guiding layers result in significant vertical confinement of the optical mode and the band structure simulations indicate the formation of a *p-n* junction resulting from polarization-induced doping. XRD and TEM studies of these structures indicate that the compositionally graded AlGaN layer may also be serving as a strain transition buffer, by blocking threading defects in the vicinity of the AlN/AlGaN heterointerface, resulting in reduction of the TDs in the active layer. Polarization dependent PL studies indicate that the emitted light is strongly TM polarized (degree of polarization, 0.79), a result expected for bulk AlGaN films with 70% AlN mole fraction. Finally, electron-beam pumping of these GRINSCHs provides evidence of the onset of stimulated emission at room temperature. Future studies will focus on the formation of resonant cavity as well more efficient doping of the *p*- and *n*-layers in order to obtain electrically pumped deep UV lasers.

ACKNOWLEDGMENTS

The work was supported by the Defense Advanced Research Projects Agency CMUVT Program (PM: John Albrecht) under subcontract from Photon Systems Inc. (U.S. Army Cooperative Agreement No. W911NF-11-1-0034). The authors also acknowledge the use of facilities in the John M. Cowley Center for High Resolution Electron Microscopy at Arizona State University.

[1]S. Nakamura, "Gallium nitride I," in *Semiconductors and Semimetals*, edited by J. I. Pankove and T. D. Moustakas (Academic, New York, 1998), Vol. 50, pp. 431–457.
[2]T. D. Moustakas, "Gallium nitride II," in *Semiconductors and Semimetals*, edited by J. I. Pankove and T. D. Moustakas (Academic, New York, 1999), Vol. 57, pp. 33–121.
[3]H. Morkoc, *Handbook of Nitride Semiconductors and Devices, Vol. 3: GaN-Based Optical and Electronic Devices* (Wiley-VCH, New York, 2009).
[4]A. Khan, K. Balakrishnan, and T. Katona, Nature Photon. **2**, 77 (2008).
[5]C. Pernot *et al.*, Appl. Phys. Express **3**, 061004 (2010).
[6]H. Hirayama, Y. Tsukada, T. Maeda, and N. Kamata, Appl. Phys. Express **3**, 031002 (2010).
[7]R. Grandusky, S. R. Gibb, M. C. Mendrick, C. Moe M. Wraback, and L. J. Schowalter, Appl. Phys. Express **4**, 082101 (2011).
[8]M. Shatalov *et al.*, Appl. Phys. Express **5**, 082101 (2012).
[9]M. R. Krames, O. B. Shchekin, R. Mueller-Mach, G. O. Mueller, L. Zhou, G. Harbers, and M. G. Craford, J. Display Technol. **3**, 160 (2007).
[10]T. Takano, Y. Narita, A. Horiuchi, and H. Kawanishi, Appl. Phys. Lett. **84**, 3567 (2004).
[11]T. Wunderer, C. L. Chua, Z. Yang, J. E. Northrup, N. M. Johnson, G. A. Garrett, H. Shen, and M. Wraback, Appl. Phys. Express **4**, 092101 (2011).
[12]E. F. Pecora, W. Zhang, A. Yu. Nikiforov, L. Zhou, D. Smith, J. Yin, R. Paiella, L. Dal Negro, and T. D. Moustakas, Appl. Phys. Lett. **100**, 061111 (2012).
[13]E. F. Pecora, W. Zhang, J. Yin, R. Paiella, L. Dal Negro, and T. D. Moustakas, Appl. Phys. Express **5**, 032103 (2012).
[14]P. Kozodoy, H. Xing, S. P. DenBaars, U. K. Mishra, A. Saxler, R. Perrin, S. Elhamri, and W. C. Mitchel, J. Appl. Phys. **87**, 1832 (2000).
[15]Y. Taniyasu, M. Kasu, and T. Makimoto, Nature **441**, 325(2006).
[16]H. Yoshida, Y. Yamashita, M. Kuwabara, and H. Kan, Nature Photon. **2**, 551 (2008).
[17]H. Yoshida, Y. Yamashita, M. Kuwabara, and H. Kan, Appl. Phys. Lett. **93**, 241106 (2008).
[18]A. Salvador, W. Kim, Ö. Aktas, A. Botchkarev, Z. Fan, and H. Morkoc, Appl. Phys. Lett. **69**, 2692 (1996).
[19]A. Janotti, E. Snow, and C. G. Van de Walle, Appl. Phys. Lett. **95**, 172109 (2009).
[20]P. Kozodoy, M. Hansen, S. P. DenBaars, and U. K. Mishra, Appl. Phys. Lett. **74**, 3681 (1999).
[21]P. Kozodoy, Y. P. Smorchkova, M. Hansen, H. Xing, S. P. DenBaars, U. K. Mishra, A. W. Saxler, R. Perrin, and W. C. Mitchel, Appl. Phys. Lett. **75**, 2444 (1999).
[22]M. L. Nakarmi, K. H. Kim, J. Li, J. Y. Lin, and H. X. Jiang, Appl. Phys. Lett. **82**, 3041 (2003).
[23]J. Simon, V. Protasenko, C. Lian, H. Xing, and D. Jena, Science **327**, 60 (2010).
[24]J. Verma, J. Simon, V. Protasenko, T. Kosel, H. G. Xing, and D. Jena, Appl. Phys. Lett. **99**, 171104 (2011).
[25]L. Zhang *et al.*, Appl. Phys. Lett. **97**, 062103 (2010).
[26]S. Li, M. Ware, J. Wu, P. Minor, Z. Wang, Z. Wu, Y. Jiang, and G. J. Salamo, Appl. Phys. Lett. **101**, 122103 (2012).
[27]W. T. Tsang, Appl. Phys. Lett. **39**, 786 (1981).
[28]W. T. Tsang, Appl. Phys. Lett. **40**, 217 (1982).
[29]D. Kasemset, C.-S. Hong, N. B. Patel, and P. D. Dapkus, IEEE J. Quantum Electron. **QE-19**, 1025 (1983).
[30]H. Okumura, T. Kimoto, and J. Suda, Appl. Phys. Express **4**, 025502 (2011).
[31]H. Okumura, T. Kimoto, and J. Suda, Phys. Status Solidi C **7**, 2094 (2010).
[32]Theodore D. Moustakas, ECS Trans. **41**, 3 (2011).
[33]Theodore D. Moustakas, Phys. Status Solidi A **210**, 169 (2013).
[34]T. D. Moustakas, IEEE 2012 Lester Eastman Conference on High Performance Devices-IEEE Xplore (in press).
[35]T. D. Moustakas and A. Bhattacharyya, ECS Trans. **35**, 63 (2011).
[36]T. D. Moustakas and A. Bhattacharyya, Phys. Status Solidi C **9**, 580 (2012).
[37]A. Bhattacharyya, T. D. Moustakas, L. Zhou, D. J. Smith, and W. Hug, Appl. Phys. Lett. **94**, 181907 (2009).
[38]Y. Liao, C. Thomidis, C. K. Kao, and T. D. Moustakas, Appl. Phys. Lett. **98**, 081110 (2011).
[39]T. D. Moustakas, Y. Liao, C. K. Kao, C. Thomidis, A. Bhattacharyya, D. Bhattarai, and A. Moldawer, Proc. SPIE **8278**, 82780L-1 (2012).

[40]W. Zhang *et al.*, J. Vac. Sci. Technol. B **30**, 02B119 (2012).
[41]D. Brunner, H. Angerer, E. Bustarret, F. Freudenberg, R. Hopler, R. Dimitrov, O. Ambacher, and M. Stutzmann, J. Appl. Phys. **82**, 5090 (1997).
[42]H. Yoshida, M. Kuwabara, Y. Yamashita, Y. Takagi, K. Uchiyama, and H. Kan, New J. Phys. **11**, 125013 (2009).
[43]R. Dalmau *et al.*, J. Electrochem. Soc. **158**, H530 (2011).
[44]K. B. Nam, J. Li, M. L. Nakarmi, J. Y. Lin, and H. X. Jiang, Appl. Phys. Lett. **84**, 5264 (2004).
[45]E. F. Pecora and H. Sun, "Large optical gain on AlGaN based GRINSCH structure," Appl. Phys. Lett. (to be published).